60 A/W high voltage GaN avalanche photodiode demonstrating robust avalanche and high gain up to 525 K

Cite as: Appl. Phys. Lett. **116**, 211102 (2020); doi: 10.1063/1.5140005 Submitted: 24 November 2019 · Accepted: 6 May 2020 · Published Online: 27 May 2020







Dong Ji, 1, a) Dong Ji, 1, a) Dong Ji, 1, a) Burcu Ercan, 2 Garrett Benson, 3 A. K. M. Newaz, 3 D and Srabanti Chowdhury 1, 2, a) Dong Ji, 1, a) Dong Ji, 1,

AFFILIATIONS

- Department of Electrical Engineering, Stanford University, Stanford, California 94305, USA
- ²Department of Electrical and Computer Engineering, University of California, Davis, California 95616, USA
- ³Department of Physics and Astronomy, San Francisco State University, San Francisco, California 94132, USA

ABSTRACT

This paper presents a demonstration of a 278 V GaN avalanche photodiode offering a photoresponsivity of 60 A/W and capable of operating at high temperature with a high gain of 10^5 . The GaN n-i-p diode fabricated on a free-standing GaN substrate showed robust avalanche, which has not been observed on any GaN avalanche photodiodes (APDs) grown on foreign substrates. Both electrical and optical characterization studies were conducted to validate the occurrence of avalanche in these devices. The device showed a positive temperature coefficient of breakdown voltage, which follows the nature of avalanche breakdown. The positive coefficient was measured to be $3.85 \times 10^{-4} \text{ K}^{-1}$ (0.1 V/K) at a measurement temperature ranging from 300 K to 525 K. The avalanche-induced electroluminescence is also reported here in GaN APDs. The diode demonstrated superior performance by simultaneously offering a high photoresponsivity of 60 A/W, a high gain of 10^5 up to 525 K, and low dark current $(1.5 \times 10^{-5} \text{ A/cm}^2)$, measured at $0.95 \times \text{BV}$ following industry standards.

Published under license by AIP Publishing. https://doi.org/10.1063/1.5140005

High-gain ultraviolet (UV) detectors are significant for various applications, such as medicine, defense, and optical communication. III-Nitrides are attractive as UV detectors as avalanche photodiodes (APDs) due to their appropriate bandgap energy, but more so for the bandgap engineering flexibility in III-nitride materials. However, unlike in conventional III-V, Si, and SiC didoes, where avalanche is a well-established phenomenon, it was missing in GaN diodes until 2013. Although UV photodiodes have been reported, there was no demonstration of avalanche capability in those GaN photodiodes.

GaN epitaxial layers are typically grown on foreign substrates, such as sapphire, silicon carbide, and silicon. Due to the large lattice mismatch between GaN and these foreign substrates, GaN epitaxial layers exhibit high dislocation densities on the order of 10^8 – 10^9 cm⁻², which inhibits the avalanche process, and therefore, most breakdowns in these devices are catastrophic.

The homogeneous GaN films grown on free-standing GaN substrates enable low dislocation densities on the order of 10⁵ cm⁻², which is 3–4 orders lower than those of GaN on foreign substrates. In GaN electronics, the use of low defect density GaN combined with an appropriate electric field mitigation technique, such as ion implanted

edge termination, bevel termination, and ion-compensated moat etch termination, has demonstrated avalanche in pn junction diodes.

In this study, we designed an APD based on the GaN n–i–p diode structure grown on a single crystalline, low defect density GaN substrate. A robust avalanche capability was demonstrated with a buried p-GaN design, using an activation p-GaN technique and an ionimplanted edge termination. The APD exhibited an extremely low dark current of 1.5×10^{-5} A/cm² and a high gain above 10^5 . Moreover, the device performed remarkably well up to 525 K, demonstrating such high temperature performance.

The n–i–p diode used in this study is shown in Fig. 1(a). The epitaxial structure began with growing a $1-\mu m$ -thick p+GaN layer ([Mg]: $4\times 10^{19}~{\rm cm}^{-3}$) on top of the free standing GaN substrate. After the UV Ozone and HF treatment, a $1-\mu m$ -thick n-GaN drift layer and a 200-nm-thick n+GaN layer ([Si]: $5\times 10^{18}~{\rm cm}^{-3}$) were grown on top of the p+GaN by metal organic chemical vapor deposition (MOCVD). By using the UV Ozone and HF treatment, the residual impurities (Si, C, and O) at the regrowth interface could be removed effectively $^{10-12}$ and this was confirmed by C–V and SIMS analyses. During the MOCVD growth, the Mg ions in the buried p+GaN were

a) Authors to whom correspondence should be addressed: dongji@stanford.edu and srabanti@stanford.edu

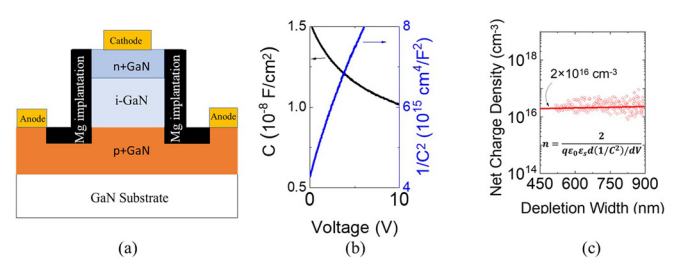


FIG. 1. (a) The schematic of the GaN avalanche photodiode (APD). Double-energy Mg-ion implantation was used to compensate the plasma damage on device sidewalls. The active region of the diode has a radius of 100 μ m. (b) C–V analysis of the photodiode. The black curve indicates the capacitance, and the blue curve indicates 1/C². The net charge density can be calculated by $n=\frac{2}{q\epsilon_0\epsilon_d d(1/C^2)/dV}$. (c) Net doping concentration in the drift region obtained by the C–V measurement. The average net doping concentration was about $2\times 10^{16}\,\mathrm{cm}^{-3}$.

passivated by hydrogen. To activate the Mg ions in the buried p+GaN, a 1.4- μ m-deep mesa was etched using Cl₂/BCl₃ gases in reactive ion etching (RIE), and then a rapid thermal annealing was performed. The buried Mg ions were activated by diffusing out hydrogen through sidewalls. The doping concentration of the n-GaN drift layer was analyzed by the C-V measurement. The net doping density in the n-GaN region was about 2×10^{16} cm⁻³. Figures 1(b) and 1(c) show the C-V characteristics and the net doping concentration.

The device edge termination was realized by a two-step Mg ion implantation: $50\,\mathrm{keV}$ (dose = $3\times10^{14}\,\mathrm{cm^{-2}}$) and $190\,\mathrm{keV}$ (dose = $1\times10^{15}\,\mathrm{cm^{-2}}$). The estimated ion implanted depth was 170 nm. The Mg ions can also compensate the plasma damage introduced by the mesa etching, which eliminated the sidewall leakage. Ni/Au metal stack was deposited for the anode electrode, and the Ti/Au metal stack was deposited for the cathode electrode.

The temperature-dependent reverse I-V characteristics are shown in Fig. 2(a). The breakdown voltage increased with the temperature with a positive temperature coefficient [as shown in Fig. 2(b)]. The temperature-dependent breakdown voltage can be written as BV $(T) = \mathrm{BV}_{300\mathrm{K}} \ (1 + \alpha \Delta T)$, where α is the temperature coefficient. By measuring the device in a temperature range of 300 K to 525 K, the temperature coefficient was $3.85 \times 10^{-4} \ \mathrm{K}^{-1}$. Figure 2(e) compares the temperature coefficients of avalanche breakdown voltage of different materials, Si, 13 GaAs, 14 InP, 15 InAlAs, 15 and 4H–SiC. 16 Although these materials have a different crystal structure and bandgap, the temperature coefficients of avalanche breakdown voltage are quite close.

A one-dimensional simulation program was developed to model the impact ionization in GaN n-i-p diodes. The simulation was based on our recently reported impact ionization coefficients [$\alpha_n = 2.11 \times 10^9 \exp(-3.689 \times 10^7/E) \text{ cm}^{-1}$ and $\alpha_p = 4.39 \times 10^6 \exp(-1.8 \times 10^7/E) \text{ cm}^{-1}$], which agrees with the Monte Carlo simulated results. From simulation of the present photodiode structure, it is found that the avalanche occurs when the junction electric field approached 3 MV/cm, and the corresponding blocking voltage was 278 V, which matches very well with the measured data. Figure 2(c) shows the comparison of the multiplication factors obtained by the measurement and simulation. From these results, it can be concluded that the device broke down by the impact ionization and not by any other catastrophe like the local electric field peaking above the critical value.

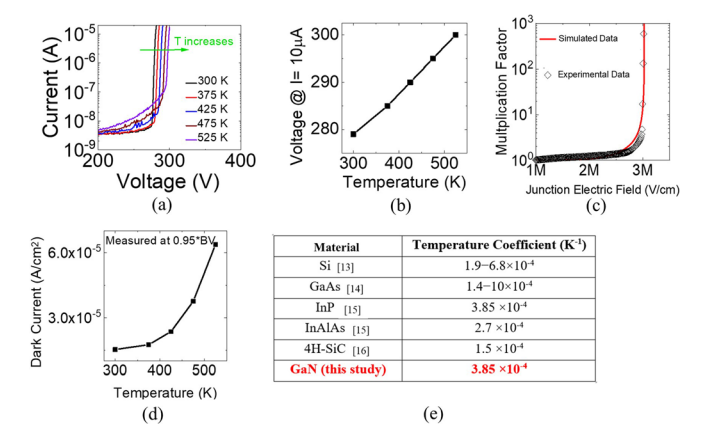


FIG. 2. (a) The measured reverse characteristics of the photodiode at different temperatures from 300 K (room temperature) to 525 K (250 °C). (b) Blocking voltage as a function of temperature. The blocking voltage increases with rising temperature in a linear manner (0.1 V/K), which follows the feature of avalanche breakdown. (c) Comparison of the simulated and measured current multiplication as a function of junction electric field. The simulated multiplication factor was calculated based on the recently reported impact ionization coefficients $[\alpha_n=2.11\times10^9 {\rm exp}(-3.689\times10^7/E)~{\rm cm}^{-1}]$. (d) The dark current as a function of the measured temperature. The definition of the breakdown voltage was the voltage when the current reached 10 $\mu{\rm A}$, and the dark current was measured at a voltage equaling 0.95 \times BV. (e) Reported temperature coefficient of avalanche breakdown of main semiconductors. $^{13-16}$

Figure 2(d) shows the dark current (measured at the voltage that equals $0.95 \times BV$ following commercial device measurement standards as a function of measurement temperature). The temperature coefficient of the dark current was 1.006 times/K, which is much lower than that of commercially available Si and InGaAs avalanche photodiodes, ^{18,19} the values of which are 1.1 times/K and 1.07 times/K, respectively. This is a key advantage offered by the large bandgap energy of GaN

Electroluminescence is another visible and obvious outcome of avalanche breakdown, especially for direct bandgap materials, and reported in GaAs.²⁰ However, to date, observation of electroluminescence has not been reported in the literature on GaN APDs.^{1–6,22–31}

In this study, electroluminescence was observed, further confirming the avalanche process in the GaN APDs. Figures 3(b) and 3(c) show the optical microscope image of the device with electroluminescence when the device was in a controlled avalanche breakdown with different avalanche current levels. The electroluminescence has a peak wavelength of 410 nm, which matches with the reported electroluminescence of the forward biased GaN LED with a Mg-related recombination center;²¹ this can be explained as the diffusion of Mg from the p+GaN layer into the top layers, creating recombination centers. Figure 3(e) shows the schematic illustration of the carrier multiplication and recombination processes during the avalanche.

The photoresponsivity of the device is shown in Fig. 4(a). The device has a peak responsivity for the wavelength ranging from 350 nm to 370 nm, which corresponded to the energy bandgap of GaN. The photoresponsivity reduced sharply for wavelengths exceeding 370 nm. The peak photoresponsivity was 0.24 A/W when the device is not in the avalanche regime, corresponding to a quantum efficiency (QE) of 80%. When a reverse bias was applied on the device,

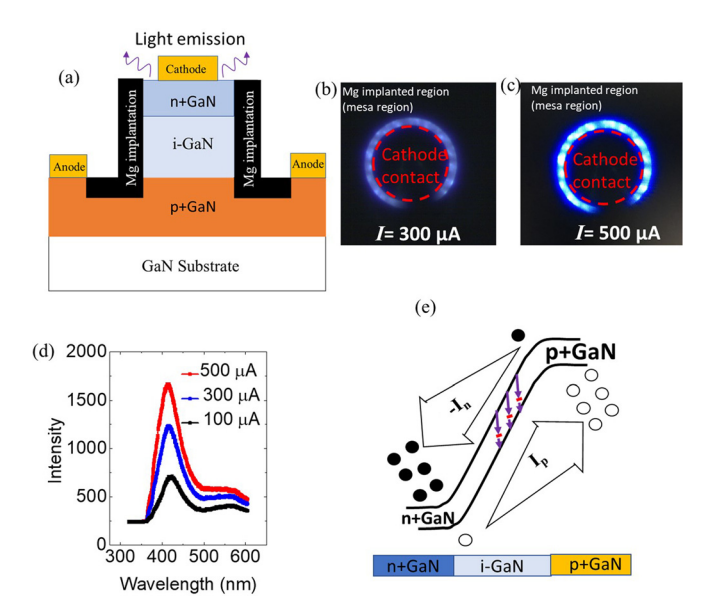


FIG. 3. (a) Cross-sectional schematic of the diode, where the light emission was observed in the top n+GaN open space. (b) and (c) Microscope images of the electroluminescence of the photodiode with different avalanche currents of 300 μ A and 500 μ A. (d) The spectrum of the electroluminescence. (e) Schematic illustration of the carrier multiplication and recombination during the avalanche. The recombination of electrons and holes generates photons; therefore, electroluminescence can be observed.

the photoresponsivity increased as the impact ionization occurred, as shown in Fig. 4(b). Under a reverse bias of 280 V, a record high photoresponsivity of 60 A/W was obtained.

Figure 4(c) shows the ultraviolet light-induced current (I_{UV}) and dark current (I_{Dark}) measured at temperatures of 300 K and 525 K,

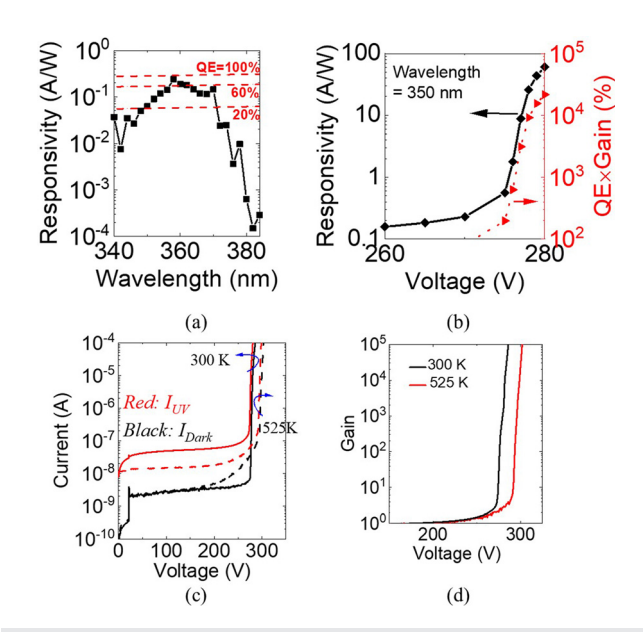


FIG. 4. (a) Responsivity of the photodiode. The peak response wavelength was from 350 nm to 370 nm. The peak quantum efficiency (QE) was about 80%. (b) Responsivity and QE as a function of reverse bias. A record high responsivity of 60 A/W was measured under a reverse bias of 280 V. (c) Reverse current measured in the dark environment and under ultraviolet light illumination ($\lambda=350$ nm). The measurement temperatures were 300 K (solid curves) and 525 K (dashed curves). (d) Optical gain of the device at 300 K and 525 K.

respectively. The measured gain of the diode was 10^5 at $300\,\mathrm{K}$ and remained constant up to 525 K, demonstrating its capability to operate at high temperature.

Table I summarizes the reported key results on avalanche photodiodes in GaN and compares with commercial Si and InGaAs

TABLE I. Summary of the reported key results on avalanche photodiodes.

	BV (V)	I _{Dark} (A/cm ² @95% BV)	Maximum responsivity (A/W)	Maximum gain	Maximum temperature (°C)	Temperature coefficient of breakdown voltage (V/°C)
This work	278	1.5×10^{-5}	60	10 ⁵	250	0.1
Hamamatsu Si APD ¹⁸	250	6×10^{-6}	55	1000	85	1.85
Hamamatsu InGaAs APD ¹⁹	65	6.3×10^{-5}	0.8	30	85	0.1
GaN-on-GaN ²²	95	5×10^{-4}	NA	1000	NA	NA
GaN-on-Sapphire ²³	90	0.044	0.163	1.9×10^4	NA	NA
GaN-on-Sapphire ²⁴	>120	1.27×10^{-4}	0.23	NA	NA	NA
GaN-on-GaN ²⁵	98	1×10^{-4}	0.61	>1000	NA	NA
GaN-on-Sapphire ²⁶	92	795	NA	300	NA	0.13
GaN-on-GaN ²⁷	92.3	2×10^{-4}	0.15	1.4×10^4	NA	NA
GaN-on-Sapphire ²⁸	NA	NA	0.11	NA	NA	NA
GaN-on-SiC ²⁹	160	2×10^{-8}	4.2	10^{5}	201	NA
AlGaN-on-GaN ³⁰	100	1×10^{-4}	0.8	8×10^5	NA	NA
AlGaN-on-Sapphire ³⁰	90	1×10^{-2}	NA	2×10^4	NA	NA
GaN-on-GaN ^{31,32}	75	2×10^{-3}	NA	2.8×10^{7}	NA	NA
Si UV APD ³³	10.8	2.5×10^{-3}	0.1	2800	NA	NA

avalanche photodiodes, which shows that the GaN avalanche photodiode presented in this study shows promising potential for commercial UV detectors. Moreover, Table I lists the reported papers on GaN APDs. Some of these studies, ^{30,31} although record high optical gains, show no evidence of avalanche breakdown, typically verified with a positive temperature coefficient. No electroluminescence has been reported in these studies.

In summary, a GaN n-i-p avalanche photodiode with remarkable performance metrics has been designed and fabricated on the free-standing GaN substrate. The device offers an avalanche breakdown at a reverse bias of 278 V with the breakdown voltage increasing with rising temperatures, a clear signature of avalanche. The dark current was 1.5×10^{-5} A/cm², and no increase in leakage current was observed until the avalanche breakdown occurred. Under the reverse bias, electroluminescence was observed when impact ionization occurred. The device showed a peak photoresponsivity at the wavelength between 350 nm and 370 nm. When the avalanche occurred (reverse bias = 280 V), the photoresponsivity was 60 A/W, which is the highest reported in GaN n-i-p photodiodes. A key feature of the device is that it can be operated at a high temperature up to 525 K (250 °C) with a gain of 10⁵. The reported gain of 10⁵ and a dark current as low as 1.5×10^{-5} A/cm² obtained from the fabricated GaNon-GaN APD confirm the demonstration of our design and device development using the GaN substrate with appropriate field management in the device.

The authors are thankful to Professor James Harris for III-As APD related discussion that helped us evaluate the performance of the reported devices. The authors would also thank Anand Vikas Lalwani and Dr. Jaeyi Chun for measurement-related help. This work was partly funded under the William George and Ida Mary Hoover Faculty Fellowship at Stanford and the ARL (No. W911NF-18-2-0017), and the responsivity was measured at Professor Newaz's lab at SFSU (No. NSF ECCS-1708907).

DATA AVAILABILITY

The data that support the findings of this study are available within this article.

REFERENCES

- ¹S. Verghese, K. A. McIntosh, R. J. Molnar, C.-L. Chen, K. M. Molvar, I. Melngailis, and R. L. Aggarwal, in Device Research Conference (1998), pp. 54–55.
- ²J. C. Carrano, D. J. Lambert, C. J. Eiting, C. J. Collins, T. Li, S. Wang, B. Yang, A. L. Beck, R. D. Dupuis, and J. C. Campbell, Appl. Phys. Lett. **76**, 924 (2000).
- ³R. McClintock, J. L. Pau, K. Minder, C. Bayram, P. Kung, and M. Razeghi, Appl. Phys. Lett. **90**, 141112 (2007).
- ⁴E. Cicek, Z. Vashaei, R. McClintock, C. Bayram, and M. Razeghi, Appl. Phys. Lett. **96**, 261107 (2010).
- ⁵Y. Zhang, S.-C. Shen, H. J. Kim, S. Choi, J.-H. Ryou, R. D. Dupuis, and B. Narayan, Appl. Phys. Lett. **94**, 221109 (2009).
- ⁶I. C. Kizilyalli, A. P. Edwards, O. Aktas, T. Prunty, and D. Bour, IEEE Trans. Electron Devices **62**(2), 414 (2015).

- ⁷T. Maeda, T. Narita, H. Ueda, M. Kanechika, T. Uesugi, T. Kachi, T. Kimoto, M. Horita, and J. Suda, in IEEE International Electron Devices Meeting (2018), pp. 687–690.
- ⁸D. Ji, S. Li, B. Ercan, C. Ren, and S. Chowdhury, IEEE Electron Device Lett. **41**, 264–267 (2020).
- ⁹P. Suvarna, J. Bulmer, J. M. Leathersich, J. Marini, I. Mahaboob, J. Hennessy, L. D. Bell, S. Nikzad, and F. Shahedipour-Sandvik, IEEE Photonics Technol. Lett. 27, 498–501 (2015).
- 10S. Chowdhury, Ph.D. dissertation, University of California, Santa Barbara, 2010.
- ¹¹D. Ji, C. Gupta, A. Agarwal, S. H. Chan, C. Lund, W. Li, S. Keller, U. K. Mishra, and S. Chowdhury, IEEE Electron Device Lett. 39, 711–714 (2018).
- ¹²I. Stricklin, M. Monavarian, A. Aragon, G. Pickrell, M. Crawford, A. Allerman, A. Armstrong, and D. Feezell, Proc. SPIE 10754, 1075402 (2018).
- ¹³R. Hall, Int. J. Electron. **22**, 513–519 (1967).
- ¹⁴C. Groves, R. Ghin, J. P. R. David, and G. J. Rees, IEEE Trans. Electron Devices 50, 2027–2031 (2003).
- ¹⁵L. J. J. Tan, D. S. G. Ong, J. S. Ng, C. H. Tan, S. K. Jones, Y. Qian, and J. P. R. David, IEEE J. Quantum Electron. 46, 1153–1157 (2010).
- ¹⁶K. V. Vassilevski, K. Zekentes, A. V. Zorenko, and L. P. Romanov, IEEE Electron Device Lett. 21, 485–487 (2000).
- ¹⁷D. Ji, B. Ercan, and S. Chowdhury, Appl. Phys. Lett. 115, 073503 (2019).
- 18HAMAMATSU Inc., Silicon Avalanche Photodiode S14643-2, Datasheet (HAMAMATSU, Inc., 2019).
- ¹⁹HAMAMATSU Inc., InGaAs Avalanche Photodiode G14858-0020AA, Datasheet (HAMAMATSU Inc., 2019).
- ²⁰M. Lahbabi, A. Ahaitouf, M. Fliyou, E. Abarkan, J. P. Charles, A. Bath, A. Hoffmann, S. E. Kerns, and D. V. Kerns, Jr., J. Appl. Phys. 95, 1822–1828 (2004)
- ²¹I. Akasaki, H. Amano, M. Kito, and K. Hiramatsu, J. Lumin. 48–49, Pt. 2, 666–670 (1991).
- ²²J. B. Limb, D. Yoo, J. H. Ryou, W. Lee, S. C. Shen, R. D. Dupuis, M. L. Reed, C. J. Collins, M. Wraback, D. Hanser, E. Preble, N. M. Williams, and K. Evans, Appl. Phys. Lett. 89, 011112 (2006).
- ²³C. Bayram, J. L. Pau, R. McClintock, M. Razeghi, M. P. Ulmer, and D. Silversmith, Appl. Phys. Lett. 93, 211107 (2008).
- ²⁴B. Butun, T. Tut, E. Ulker, T. Yelboga, and E. Ozbay, Appl. Phys. Lett. **92**, 033507 (2008).
- ²⁵R. D. Dupuis, J. Ryou, S. Shen, P. D. Yoder, Y. Zhang, H. J. Kim, S. Choi, and Z. Lochner, J. Cryst. Growth 310, 5217–5222 (2008).
- ²⁶S. Verghese, K. A. McIntosh, R. J. Molnar, L. J. Mahoney, R. L. Aggarwal, M. W. Geis, K. M. Molvar, E. K. Duerr, and I. Melngailis, IEEE Trans. Electron Devices 48(3), 502–511 (2001).
- ²⁷S. C. Shen, Y. Zhang, D. Yoo, J. B. Limb, J. H. Ryou, P. D. Yoder, and R. D. Dupuis, IEEE Photonics Technol. Lett. 19(21), 1744–1746 (2007).
- ²⁸ M. C. Chen, J. K. Sheu, M. L. Lee, C. J. Tun, and G. C. Chi, Appl. Phys. Lett. 89, 183509 (2006).
- ²⁹Q. Zhou, D. C. McIntosh, Z. Lu, J. C. Campbell, A. Sampath, H. Shen, and M. Wraback, Appl. Phys. Lett. 99, 131110 (2011).
- ³⁰J. Kim, M. Ji, T. Detchprohm, R. Dupuis, J. Ryou, A. K. Sood, N. D. Dhar, and J. Lewis, Appl. Phys. Express 8(12), 122202 (2015).
- ³¹ M. Ji, H. Jeong, M. Bakhtiary-Noodeh, S.-C. Shen, T. Detchprohm, A. K. Sood, P. P. Ghuman, S. Babu, N. K. Dhar, J. Lewis, and R. D. Dupuis, Proc. SPIE 10918, 1091814 (2019).
- ³²A. K. Sood, J. W. Zeller, P. Ghuman, S. Babu, N. K. Dhar, S. Ganguly, A. W. Ghosh, and R. D. Dupuis, Proc. SPIE 11151, 1115113 (2019).
- ³³Z. Xia, K. Zang, D. Liu, M. Zhou, T.-J. Kim, H. Zhang, M. Xue, J. Park, M. Morea, J. H. Ryu, T.-H. Chang, J. Kim, S. Gong, T. I. Kamins, Z. Yu, Z. Wang, J. S. Harris, and Z. Ma, Appl. Phys. Lett. 111, 081109 (2017).